Physica A 441 (2016) 51–61

Contents lists available at ScienceDirect

Physica A

journal homepage: www.elsevier.com/locate/physa

Comparison study of the reactive and predictive dynamic models for pedestrian flow

Yan-Qun Jiang [a,*], Wei Zhang [b], Shu-Guang Zhou [c]

[a] Department of Mathematics, Southwest University of Science and Technology, Mianyang, Sichuan, China

[b] School of Civil Engineering and Architecture, Southwest University of Science and Technology, Mianyang, Sichuan, China

[c] China Aerodynamics Research and Development Center, Mianyang, Sichuan, China

HIGHLIGHTS

- Two higher-order dynamic models, i.e. reactive vs. predictive, for pedestrian flow are formulated and compared.
- The algorithm used to solve the two dynamic models is designed.
- Numerical results show that the two models are able to reproduce the formation of stop-and-go waves and the blocking effect at bottlenecks.
- The patterns of the local structured clusters are distinctly different at bottlenecks due to different path-choice behaviors of pedestrians.
- The strong anticipation consciousness of pedestrians to compression can avoid congestion and thereby reduce accidents in pedestrian traffic.

ARTICLE INFO

Article history:
Received 2 March 2015
Received in revised form 27 July 2015
Available online 8 September 2015

Keywords:
Pedestrian flow
Reactive dynamic user-equilibrium
Predictive dynamic user-equilibrium
Traffic instability
Stop-and-go waves

ABSTRACT

This paper formulates the reactive and predictive dynamic models for pedestrian flow and presents a comparison of the two models. The path-choice behavior of pedestrians in the reactive dynamic model is described that pedestrians tend to walk along a path with the lowest instantaneous cost. The desired walking direction of pedestrians in the predictive dynamic model is chosen to minimize the actual cost based on predictive traffic conditions. An algorithm used to solve the two models encompasses a cell-centered finite volume method for a hyperbolic system of conservation laws and a time-dependent Hamilton–Jacobi equation, a fast sweeping method for an Eikonal-type equation, and a self-adaptive method of successive averages for an arisen discrete fixed point problem. The two models and their algorithm are applied to investigate the spatio-temporal patterns of flux or density and path-choice behaviors of pedestrian flow marching in a facility scattered with an obstacle. Numerical results show that the two models are able to capture macroscopic features of pedestrian flow, traffic instability and other complex nonlinear phenomena in pedestrian traffic, such as the formation of stop-and-go waves and clogging at bottlenecks. Different path-choice strategies of pedestrians cause different spatial distributions of pedestrian density specially in the high-density regions (near the obstacle and exits).

1. Introduction

In recent years, pedestrian traffic problems have attracted considerable attention of scientists from different fields. The study on pedestrian and crowd dynamics can help to develop guidelines for planning and designing pedestrian facilities.

* Corresponding author.
E-mail addresses: jyq2005@mail.ustc.edu.cn, yqjiang2014@126.com (Y.-Q. Jiang), zwell@mail.ustc.edu.cn (W. Zhang), zhousgcfd@sina.com (S.-G. Zhou).

http://dx.doi.org/10.1016/j.physa.2015.08.047
0378-4371/

The modeling of pedestrian crowd dynamics is generally classified into three approaches: the microscopic, mesoscopic and macroscopic modeling approaches. The microscopic modeling approach focuses on the details of features of pedestrian movement and the behavior characteristics of each individual in a crowd. Microscopic models mainly encompass discrete space models (e.g. cellular automaton models [1–4] and lattice gas models [5–8]) which allow pedestrians to walk at or within a fixed note or grid and update the current positions at discrete time intervals, and continuous space models (e.g. social force models [9–11]) which allow pedestrians to move continuously within a pre-defined geometry [12]. Most microscopic models can reveal many interesting phenomena in pedestrian dynamics, e.g. clustering or queuing at bottlenecks, stripe formation and chevron effect [13,14]. Mesoscopic models like gas-kinetic models [15–18] are built based on the mathematical kinetic theory for active particles and have the ability to retain various complexity features of crowds viewed as a living system. For example, pedestrian fundamental diagrams may be generated by individual-based interactions based on kinetic theory methods [19,20]. In the mesoscopic equations, the state of the system is identified by the position and velocity of the microscopic entities, but their representation is given by a suitable probability distribution over the microscopic state [15,16]. This type of models can describe the evolution of this distribution function by introducing numerous undetermined parameters and using nonlinear integro-differential equations. Therefore, they are suitable for a small-scale environment in which the number of individual entities is not large enough to allow the use of continuous distribution functions within the framework of the mathematical kinetic theory [15].

The modeling and simulation of complex crowd movement based on microscopic and mesoscopic models generally increase the computational complexity and model parameters with the increase of the scale of individuals. In the case of a large group of pedestrians, the movement of pedestrians should behave very similar to gas particles and thus pedestrians in a large group can be treated as a flowing continuum [21]. Therefore, the macroscopic modeling approach has been extensively concerned. So far only a few of macroscopic models for unidirectional and bi-directional pedestrian flows are proposed to investigate macroscopic features of crowd movement (e.g. density, speed and flow) and behavior characteristics of pedestrians on the macroscopic scale. Based on different user-equilibrium (UE) path-choice strategies of pedestrians, namely the reactive dynamic user-equilibrium (RDUE) assignment and the predictive dynamic user-equilibrium (PDUE) assignment, macroscopic models of pedestrian flow can be divided into reactive dynamic models and predictive dynamic models. In the reactive dynamic models, pedestrians tend to choose a path from origin to destination with the lowest instantaneous walking cost based on current traffic information available to them [22–26]. In the predictive dynamic models, pedestrians' path-choice behavior is described under the hypothesis that pedestrians aim to minimize the actual walking cost from/at the current position/time to the destination based on predictive traffic conditions [27–29].

Macroscopic models of pedestrian flow, which use the continuum equation to describe the evolution of traffic density, are called first-order models. The first-order models [21–26] are actually a generalization of the Lighthill–Whitham–Richards (LWR) models proposed for vehicular traffic flow [30]. Compared to the LWR models of vehicular traffic flow, macroscopic models of pedestrian flow need to capture the dynamics of pedestrians walking in a two-dimensional (2D) or three-dimensional (3D) space and the dynamics of the interactions and the overall strategy influenced by environmental conditions [31], therefore they are more complex. The first-order models are shown to be a useful tool for the planning and design of walking facilities, but they assume the existence of an equilibrium speed–density relationship (or so-called fundamental diagram) and a natural trend toward this distribution. This type of models certainly cannot reproduce non-equilibrium phase transitions and various nonlinear dynamic phenomena observed in empirical studies [32,33]. To resolve this problem in the first-order models, higher-order models [31,34,35], which are composed of the conservation of mass and the equilibrium of linear momentum for expressing the pedestrian acceleration/deceleration dynamics, have been studied in recent years for allowing the actual velocity of motion to fluctuate around the equilibrium diagram.

In this paper, we formulate the reactive and predictive dynamic models for unidirectional pedestrian flow and present a comparison of the two dynamic models. The reactive dynamic model consists of a hyperbolic system of conservation laws with relaxation and an Eikonal-type equation [34] and the predictive dynamic model is described as a hyperbolic system of conservation laws with relaxation coupled with a time-dependent Hamilton–Jacobi (HJ) equation. An algorithm used to numerically solve the two models is composed of a cell-centered finite volume method (FVM) for the hyperbolic system of conservation laws and the HJ equation, a fast sweeping method (FSM) for the Eikonal-type equation, and a self-adaptive method of successive averages (MSA) for an arisen discrete fixed point problem. A numerical experiment is carried out to investigate macroscopic features (e.g. the spatio-temporal distributions of density) and route-choice behavior characteristics of pedestrian flow walking in a 2D continuous pedestrian facility scattered with an obstacle. We also compare the patterns of spatial distributions of pedestrian densities obtained by the two dynamic models.

The present work is organized as follows. Mathematical models for pedestrian movement are presented in Section 2. Section 3 gives numerical methods used to solve these models. Section 4 presents numerical results. Section 5 is devoted to summary and discussion.

2. Mathematical formulation

We regard a large group of pedestrians walking in a 2D continuous domain denoted by Ω as a compressible continuum fluid medium. The boundary of Ω consists of inflow boundary Γ_i, outflow boundary Γ_o and solid wall boundary Γ_w. $T = [0, t_{end}]$ (in s) is the modeling period.

2.1. Pedestrian dynamic model

Based on continuum dynamics, the dynamic model for pedestrian flow in Ω can be described as the following conservation form [34]:

$$\frac{\partial Q}{\partial t} + \nabla \cdot (F, G) = S, \quad (x, y) \in \Omega,\ t \geq 0, \tag{1}$$

$$Q(\cdot, 0) = Q_0, \tag{2}$$

where

$$Q = \begin{bmatrix} \rho \\ \rho u \\ \rho v \end{bmatrix}, \qquad F = \begin{bmatrix} \rho u \\ \rho u^2 + P \\ \rho uv \end{bmatrix}, \qquad G = \begin{bmatrix} \rho v \\ \rho uv \\ \rho v^2 + P \end{bmatrix}, \qquad S = \begin{bmatrix} 0 \\ \dfrac{\rho U_e v_x - \rho u}{\tau} \\ \dfrac{\rho U_e v_y - \rho v}{\tau} \end{bmatrix}.$$

Here, $\rho(x, y, t)$ (in ped/m^2) and $\mathbf{v}(x, y, t) = (u(x, y, t), v(x, y, t))$ (in m/s) are the density and average velocity of pedestrian flow; $U_e(\rho)$ (in m/s) is the speed–density relationship representing the desired walking speed of pedestrian flow; $P(\rho)$ denotes the equivalent traffic pressure, which is expressed as an increasing function of pedestrian density and describes the response of pedestrians to compression; $\vec{v}(x, y, t) = (v_x(x, y, t), v_y(x, y, t))$ is the unit vector expressing a desired or intended direction of motion; and $\tau = 0.5$ s is a characteristic relaxation time.

The linear stability condition of the model (1) is obtained as [34]

$$\rho \|(U_e(\rho)\vec{v})'\| \leq c(\rho), \tag{3}$$

where $c(\rho) = \sqrt{P'(\rho)}$ (in m/s) is the equivalent traffic sonic speed describing the propagating speed of small perturbation in pedestrian flow. When the condition of stability (3) is violated, traffic becomes unstable, which reproduces other kinds of complex traffic phenomena, such as the formation of jams, stop-and-go waves and other nonlinear dynamical phenomena as observed in empirical crowd flows [32,33]. The eigenvalues of the composite Jacobian matrix $\frac{\partial F}{\partial Q} n_x + \frac{\partial G}{\partial Q} n_y$ in an arbitrary spatial direction (n_x, n_y) are

$$\{(un_x + vn_y) \pm c(\rho)(n_x + n_y), un_x + vn_y\}. \tag{4}$$

Therefore, the system (1) is hyperbolic and isotropic since $(un_x + vn_y) \leq \max\{(un_x + vn_y) \pm c(\rho)(n_x + n_y)\}$. The isotropic nature of the model means that pedestrians are equally affected by mechanical cues coming from all directions.

2.2. Desired direction of motion

The governing equations for pedestrian flow (1) are complete as long as the unit vector $\vec{v}$ in the source term is specified. The determination of the desired direction of motion reflects the path-choice behavior of pedestrians in the 2D continuous region. Let $C(x, y, t)$ (in s/m) be the local walking cost distribution, which represents the walking cost per unit distance of movement incurred by pedestrians at location $(x, y) \in \Omega$ and time t. The minimum instantaneous or actual cost incurred by pedestrians walking from the current position $(x, y) \in \Omega$ at time t to the final destination is denoted by $\Phi(x, y, t)$. The desired or intended walking direction of pedestrians $\vec{v}$ is determined based on the current traffic conditions that are available at the time of making decisions or the predictive information through experience and is defined as [22,29]

$$\vec{v}(x, y, t) = -\frac{\nabla \Phi(x, y, t)}{\|\nabla \Phi(x, y, t)\|}. \tag{5}$$

For first-order macroscopic models [22,29], pedestrians or travelers always match along a minimum-cost path at the optimal average speed and thus traffic flow is always in the UE state. Therefore, these models cannot capture non-equilibrium phase transitions and various nonlinear dynamic phenomena.

For the RDUE assignment, pedestrians move in a reactive user-optimal manner and thus $\Phi(x, y, t)$ (in s) in Eq. (5) represents the lowest instantaneous cost incurred by pedestrians from the origin $(x, y) \in \Omega$ at time t to the final destination Γ_o, where $\Phi(x, y, t) = 0$, $t \in T$. Accordingly, the instantaneous cost potential $\Phi(x, y, t)$ satisfies an Eikonal-type equation [34]

$$\begin{cases} \|\nabla \Phi(x, y, t)\| = C(x, y, t), & (x, y) \in \Omega, \\ \Phi(x, y, t) = 0, & (x, y) \in \Gamma_o. \end{cases} \tag{6}$$

The two conditions (5) and (6) incorporated into Eq. (1) can guarantee pedestrians tend to walk along a path with the lowest instantaneous cost.

For the PDUE assignment, $\Phi(x, y, t)$ (in s) in Eq. (5) describes the lowest actual cost incurred by pedestrians walking from the origin $(x, y) \in \Omega$ at time t to the final destination Γ_o, where $\Phi(x, y, t) = 0$, $t \in T$. Here, the actual cost potential $\Phi(x, y, t)$ satisfies a time-dependent HJ equation [29]

$$\frac{\partial \Phi(x, y, t)}{\partial t} = U_e(\rho)(\|\nabla \Phi(x, y, t)\| - C(x, y, t)). \tag{7}$$

The two conditions (5) and (7) incorporated into Eq. (1) can guarantee that pedestrians are inclined to walk along a path with the lowest actual cost. Without loss of generality, we assume that all pedestrians have left the modeling domain at $t = t_{end}$. The traffic state at $t = t_{end}$ is considered to be static and the walking cost from location $(x, y) \in \Omega$ to the destination Γ_o is thus the instantaneous cost. Consequently, the cost potential $\Phi(x, y, t_{end})$ satisfies the following Eikonal-type equation:

$$\|\nabla\Phi(x, y, t_{end})\| = C(x, y, t_{end}). \tag{8}$$

The reactive dynamic model presented by Jiang et al. [34] for pedestrian flow now is formulated as the hyperbolic system (1) coupled with the Eikonal-type equation (6). The predictive dynamic model is formulated as the hyperbolic system (1) coupled with the HJ equation

$$\begin{cases} \dfrac{\partial\Phi}{\partial t} = U_e(\rho)(\|\nabla\Phi\| - C), \quad (x, y) \in \Omega, \\ \|\nabla\Phi(x, y, t_{end})\| = C(x, y, t_{end}), \quad (x, y) \in \Omega, \\ \Phi = 0, \quad (x, y) \in \Gamma_o. \end{cases} \tag{9}$$

3. Numerical scheme

From Section 2, in the predictive dynamic model the initial condition of the HJ equation (7) is obtained at $t = t_{end}$, as opposed to that of Eq. (1) which is given at $t = 0$. The difficulty about the numerical computation of this model is that we cannot solve Eqs. (1) and (7) together as usual. To solve this problem, we use a first-order cell-centered FVM to solve Eqs. (1) and (7), the FSM to solve Eqs. (6) and (8), and the self-adaptive MSA to solve the generated discrete fixed-point problem.

3.1. Cell-centered FVM

The treatment of the source term in Eq. (1) involves a fractional step method [36], by which each time step Δt is split into three steps. We split the system (1) into two equations, i.e. ordinary differential equations (ODEs) and partial differential equations (PDEs).

$$\text{ODEs:} \quad \frac{\mathrm{d}Q}{\mathrm{d}t} = S, \tag{10}$$

$$\text{PDEs:} \quad \frac{\partial Q}{\partial t} + \nabla \cdot (F, G) = 0. \tag{11}$$

The point values Q_{ij}^{n+1} at the $(n + 1)$th time step are obtained from Q_{ij}^{n} at the nth time step as follows. First, we update Q^n with $\tilde{Q}$ by applying a classical implicit Euler method to Eq. (10) with the time increment $\Delta t/2$. Second, we update $\tilde{Q}$ with $\bar{Q}$ by applying a cell-centered FVM to Eq. (11) with the time increment Δt. Finally, we update $\bar{Q}$ with Q^{n+1} by applying the implicit Euler method to Eq. (10) with the time increment $\Delta t/2$.

The first-order cell-centered finite volume scheme for Eq. (1) is written as

$$\begin{aligned} \tilde{Q}_{ij} &= Q_{ij}^{n} + \frac{1}{2}\Delta t S(\tilde{Q}_{ij}, \vec{v}_{ij}^{n}), \\ \bar{Q}_{ij} &= \tilde{Q}_{ij} - \frac{\Delta t}{h}\left[\left(\hat{F}_{i+\frac{1}{2}j} - \hat{F}_{i-\frac{1}{2}j}\right) + \left(\hat{G}_{ij+\frac{1}{2}} - \hat{G}_{ij-\frac{1}{2}}\right)\right], \\ Q_{ij}^{n+1} &= \bar{Q}_{ij} + \frac{1}{2}\Delta t S(Q_{ij}^{n+1}, \vec{v}_{ij}^{n}). \end{aligned} \tag{12}$$

Here, h is the mesh size in x and y dimensions and $\hat{F}_{i\pm\frac{1}{2}j}$, $\hat{G}_{i\pm\frac{1}{2}j}$ are the local Lax–Friedrichs numerical fluxes in the x- and y-directions, respectively.

$$\hat{F}_{i+\frac{1}{2}j} = \frac{1}{2}[F(\tilde{Q}_{ij}) + F(\tilde{Q}_{i+1j}) - \alpha_x(\tilde{Q}_{i+1j} - \tilde{Q}_{ij})], \tag{13}$$

$$\hat{G}_{ij+\frac{1}{2}} = \frac{1}{2}[G(\tilde{Q}_{ij}) + G(\tilde{Q}_{ij+1}) - \alpha_y(\tilde{Q}_{ij+1} - \tilde{Q}_{ij})], \tag{14}$$

where $\alpha_x = \max_{i,i+1}\{u_{ij} \pm c_{ij}\}$ and $\alpha_y = \max_{j,j+1}\{v_{ij} \pm c_{ij}\}$.

We define $H = U_e(\|\nabla\Phi\| - C)$ and the first-order cell-centered finite volume scheme for Eq. (7) is given by

$$\Phi_{ij}^{n} = \Phi_{ij}^{n+1} - \Delta t\hat{H}[(\Phi_x)_{ij}^{-}, (\Phi_x)_{ij}^{+}, (\Phi_y)_{ij}^{-}, (\Phi_y)_{ij}^{+}], \tag{15}$$

where $(\Phi_x)_{ij}^{\pm}$, $(\Phi_y)_{ij}^{\pm}$ are the right/left derivatives of Φ^{n+1} with respect to x and y, respectively. $\hat{H}$ in (15) is the Lax–Friedrichs numerical flux, which is defined as

$$\hat{H}(u^-, u^+, v^-, v^+) = H\left(\frac{u^- + u^+}{2}, \frac{v^- + v^+}{2}\right) - \frac{1}{2}[\alpha_x^H(u^+ - u^-) + \alpha_y^H(v^+ - v^-)].$$

Here, $\alpha_x^H = \max_{ij} \frac{\partial H}{\partial \Phi_x}$ and $\alpha_y^H = \max_{ij} \frac{\partial H}{\partial \Phi_y}$.

3.2. Self-adaptive MSA

We define the numerical solutions of Eqs. (12) and (15) at each grid point and each time level as $\vec{\rho}$ and $\vec{\Phi}$, respectively.

$$\vec{\rho} = \{\rho_{ij}^n,\ i = 1, 2, \ldots, I,\ j = 1, 2, \ldots, J,\ n = 1, 2, \ldots, N\},$$

$$\vec{\Phi} = \{\Phi_{ij}^n,\ i = 1, 2, \ldots, I,\ j = 1, 2, \ldots, J,\ n = 1, 2, \ldots, N\},$$

where I, J, N are the number of grid points in the x-, y- and t-directions, respectively. With a given vector $\vec{\Phi}^{old}$, we can solve Eq. (1) by (12) from $t = 0$ to $t = t_{end}$ and thus obtain the vector $\vec{\rho}$. This computation step can be described as $\vec{\rho} = \mathbf{g}(\vec{\Phi}^{old})$. With the obtained vector $\vec{\rho}$, we can update the vector $\vec{\Phi}^{old}$ with Φ^{new} based on (15) from $t = t_{end}$ to $t = 0$. This computation step can be described as $\Phi^{new} = \mathbf{h}(\vec{\rho})$. We consider the two computation steps as one iteration and denote it as

$$\vec{\Phi}^{new} = \mathbf{h}(\mathbf{g}(\vec{\Phi}^{old})) = \mathbf{f}(\vec{\Phi}^{old}).$$

With the definitions of one iteration and the function $\mathbf{f}$, we obtain a fixed-point problem

$$\vec{\Phi} = \mathbf{f}(\vec{\Phi}), \tag{16}$$

which can be solved by the MSA [29].

The initial value $\vec{\Phi}^1$ of the fixed-point problem (16) is chosen as the numerical solution of the reactive dynamic model at each grid point and each time level. With the calculation of Eq. (6) at each time step t^n by the FSM [37], we can obtain Φ^n and then compute ρ^n by (12) from $t = 0$ to $t = t_{end}$. Therefore, we obtain the density vector $\vec{\rho}^1$ and the initial value $\vec{\Phi}^1$. Note that $\vec{\rho}^1$ stores the solution of the reactive dynamic model composed of Eqs. (1) and (6) from $t = 0$ to $t = t_{end}$. By computing (15) from $t = t_{end}$ to $t = 0$ with $\vec{\rho}^1$, we obtain a temporary vector $\vec{y}^1 = \mathbf{h}(\vec{\rho}^1)$ and set $\vec{\Phi}^2 = \vec{y}^1$. Given the solution vector $\vec{\Phi}^k (k = 2, 3, \ldots)$, compute $\vec{\rho}^k, \vec{y}^k$ by

$$\vec{\rho}^k = \mathbf{g}(\vec{\Phi}^k), \qquad \vec{y}^k = \mathbf{h}(\vec{\rho}^k) = \mathbf{f}(\vec{\Phi}^k),$$

and then update the solution vector $\vec{\Phi}^{k+1}$ by

$$\vec{\Phi}^{k+1} = (1 - \lambda_k)\vec{\Phi}^k + \lambda_k \vec{y}^k.$$

Stop the iteration process if $\|\vec{\Phi}^{k+1} - \vec{\Phi}^k\|_2 \le \varepsilon$ with a given convergence threshold value $\varepsilon = 10^{-3}$. Here, λ_k is the self-adaptive step size determined as [29] to assure convergence.

4. Numerical experiments

A large group of pedestrians are assumed to walk through a rectangular facility with area of 100 m × 50 m and its vertex on the underneath left side is taken as the coordinate origin. A square obstacle with a side of length 20 m is located at (55, 20 m). An entrance is set at $x = 0$ for $0 \le y \le 50$ and two exits at the top and bottom of the facility are set at $x = 100$ for $|y - 10| \le 5$ and $|y - 40| \le 5$, respectively. The simulated domain Ω is divided into a 100 × 50 grid.

The desired walking speed of pedestrian flow U_e in Eq. (1) is expressed by the following speed–density relationship [34,35].

$$U_e(\rho) = v_f \exp(-\gamma \rho^2), \tag{17}$$

where $\gamma = 0.075$, $v_f = 1.4$ m/s and the critical density ρ_c is about 2.58 ped/m^2. The desired walking speed U_e apparently decreases with the increase of local density ρ and the function $|(U_e)'| = |\frac{dU_e}{d\rho}|$ reaches approximately a maximum value 0.33 at $\rho = \rho_c$. The local walking cost distribution $C(x, y, t)$ in Eqs. (6)–(8) is defined as [22]

$$C = \frac{1}{U_e(\rho)} + 0.01\rho^2, \tag{18}$$

where the term $\frac{1}{U_e(\rho)}$ expresses the major cost and the term $0.01\rho^2$ is the minor cost representing other associated costs such as a preference for avoiding high-density regions. The equivalent traffic sonic speed $c(\rho)$ in Eq. (3) is defined as [34,35]

$$c(\rho) = \sigma \rho, \tag{19}$$

where σ is the anticipation degree and represents the anticipation behavior of pedestrians to compression. Based on the linear stability condition (3), traffic instability will occur under the condition of $\left\|(U_e\vec{v})'\right\| > \sigma$.

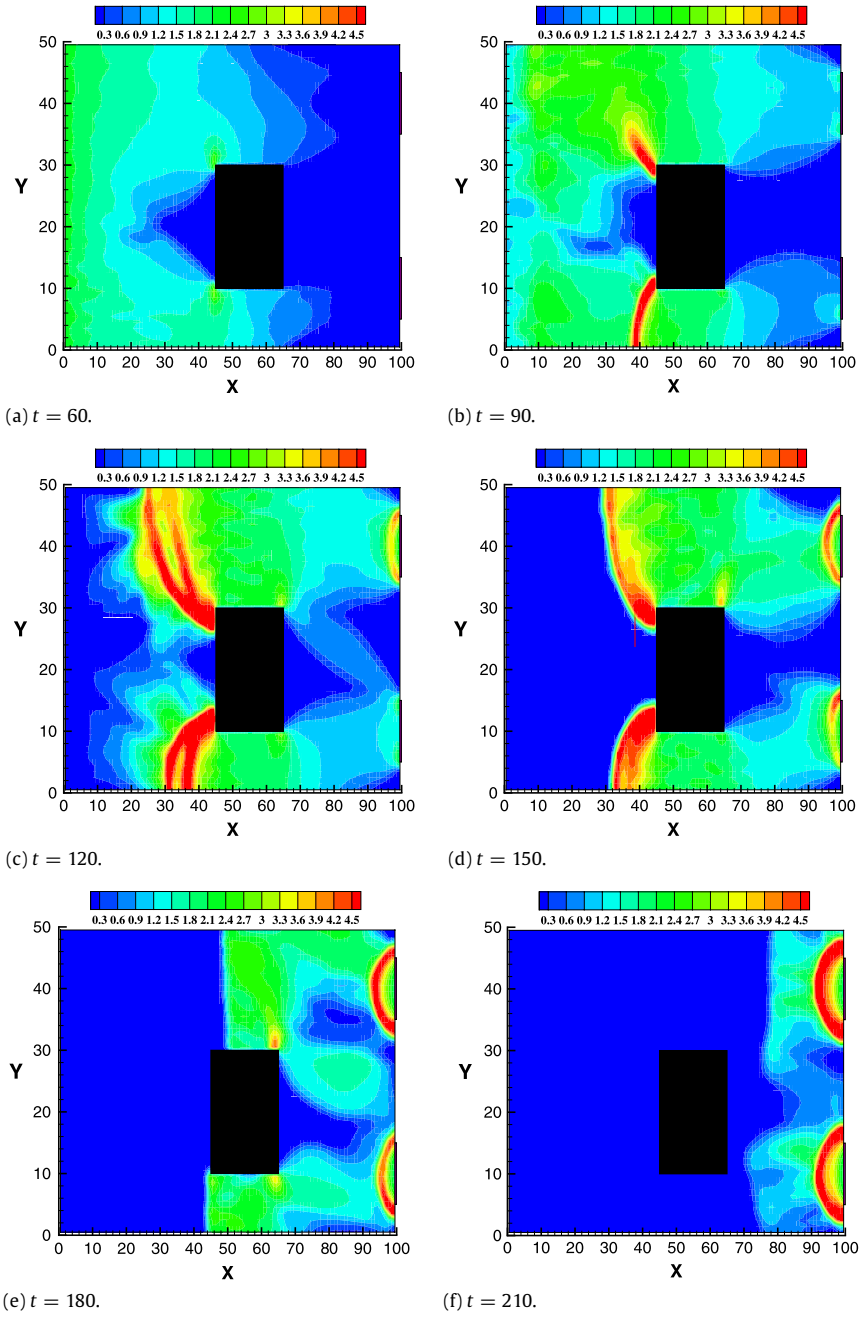

(a) $t = 60$. (b) $t = 90$.

(c) $t = 120$. (d) $t = 150$.

(e) $t = 180$. (f) $t = 210$.

Fig. 1. Density distributions at different times with $\sigma = 0.05$ based on the reactive dynamic model.

The initial and boundary conditions for the hyperbolic system (1) are described here. Initially, the walking facility is empty with $\rho_0 = 0$ ped/m^2 and $\mathbf{v}_0 = 0$ m/s. The modeling period is set to $T = [0, 300]$ and pedestrians have left the facility at the end of this period. The inflow boundary conditions on Γ_i are

$$\rho = \begin{cases} \rho_m \dfrac{t}{60}, & t \in [0, 60], \\ -\dfrac{\rho_m}{60}(t - 120), & t \in [60, 120], \\ 0, & t \in [120, 300], \end{cases} \qquad (u, v) = (U_e(\rho), 0),$$

with $\rho_m = 2.35$ ped/m^2. The outflow boundary conditions on Γ_o (i.e. two exits) are $(u, v) = (v_f, 0)$ and $\partial\rho/\partial\mathbf{n} = 0$. At the solid walls Γ_w, the free-slip and non-permeable boundary conditions are applied, i.e. $\partial\rho/\partial\mathbf{n} = 0$ and $\mathbf{v} \cdot \mathbf{n} = 0$.

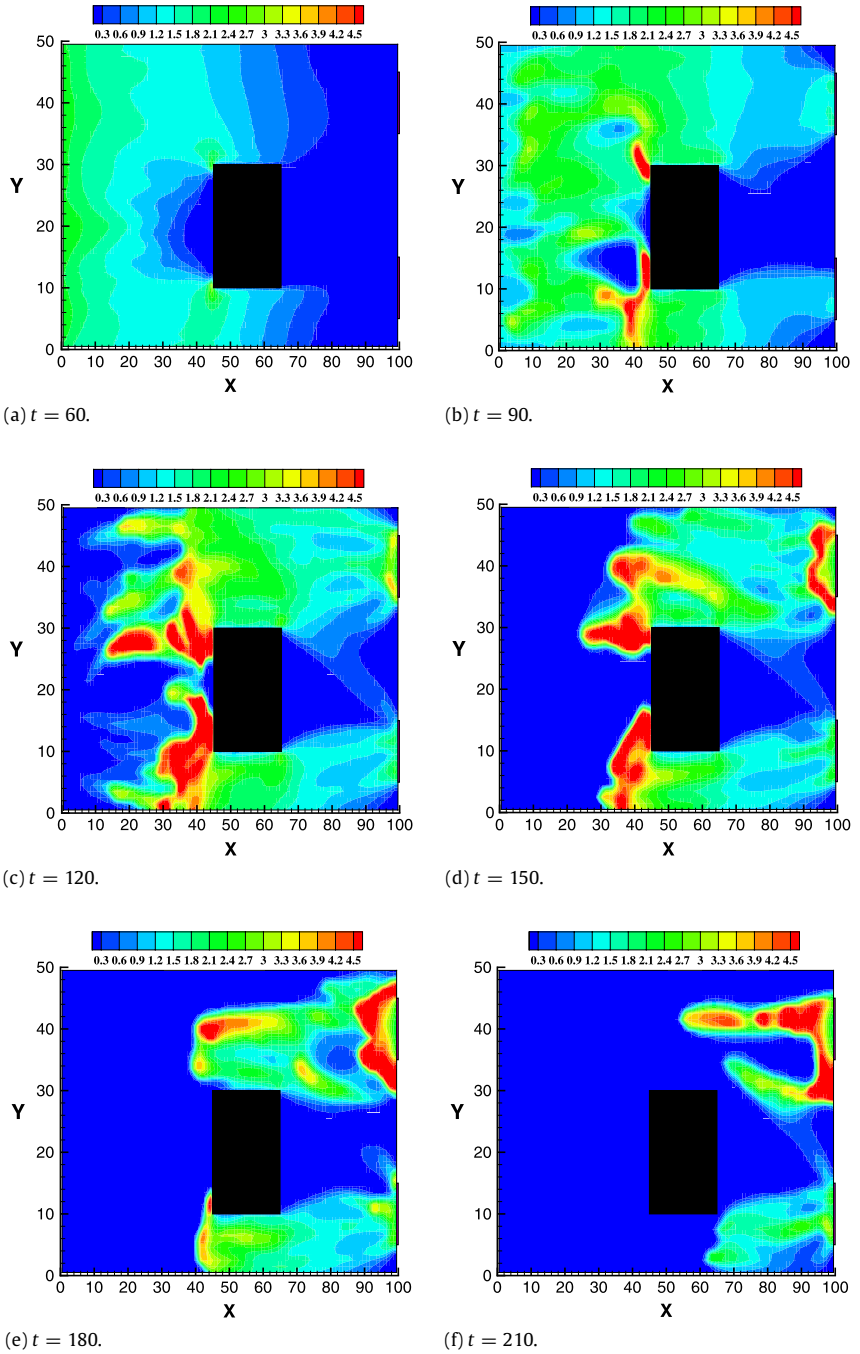

(a) $t = 60$. (b) $t = 90$.

(c) $t = 120$. (d) $t = 150$.

(e) $t = 180$. (f) $t = 210$.

Fig. 2. Density distributions at different times with $\sigma = 0.05$ based on the predictive dynamic model.

The spatial distributions of pedestrian density based on the reactive dynamic model are depicted in Fig. 1 at times $t = 60, 90, 120, 150, 180, 210$ with the anticipation degree $\sigma = 0.05$. At $t = 60$, pedestrians in a free-flow state are divided into two sub-streams by the square obstacle and a triangular vacuum region caused by the optimal path-choice strategy of pedestrians is formed on the left-hand side of this obstacle (see Fig. 1(a)). At $t = 90$, two shocks are respectively formed near the upper and lower left corners of this obstacle due to the reduction of the width of the facility and some of the pedestrians have left the facility through the exits (see Fig. 1(b)). At $t = 120$, pedestrian demand reaches its peak and more and more pedestrians gather on the left-hand side of this obstacle. Two shocks evolve into stop-and-go waves, which arises from overcrowding of the crowd and weak anticipation consciousness of pedestrians to compression (see Fig. 1(c)). In such a situation ($\sigma = 0.05 < 0.33$), traffic instability occurs and some complex dynamics of pedestrians (e.g. stop-and-go waves) can be captured by the dynamic model. At $t = 150$, the rest of pedestrians are gradually accumulated around the two

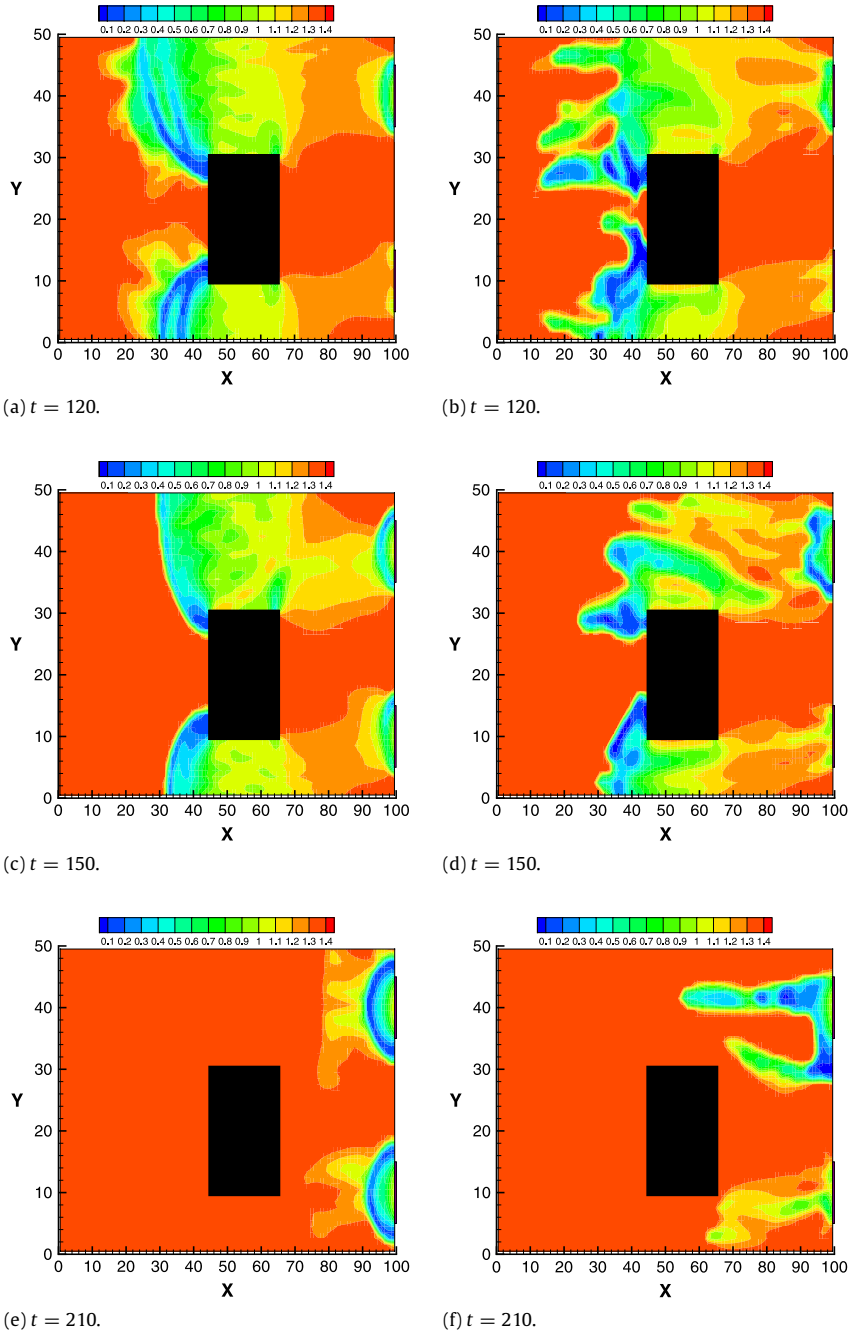

(a) $t = 120$. (b) $t = 120$.

(c) $t = 150$. (d) $t = 150$.

(e) $t = 210$. (f) $t = 210$.

Fig. 3. Desired speed at different times with $\sigma = 0.05$ based on different models (left: the reactive dynamic model; right: the predictive dynamic model).

exits of the facility (see Fig. 1(d)). At $t = 180$, we can observe the blocking phenomenon near the two exits (see Fig. 1(e)). At $t = 210$, two symmetric arch-shaped structures (e.g. clogging) are formed in front of the two exits, respectively (see Fig. 1(f)), which is caused by the RDUE path-choice behavior of pedestrians.

Fig. 2 shows the spatial distributions of pedestrian density based on the predictive dynamic model at times $t = 60, 90, 120, 150, 180, 210$ with the anticipation degree $\sigma = 0.05$. By comparing this figure with Fig. 1, we can see that the main differences exist in high-density regions (e.g. near the obstacle and the exits). Different path-choice behaviors of pedestrians result in different patterns of the spatial distributions of pedestrian density. Local structured clusters (e.g. stop-and-go waves) can also be reproduced by the predictive dynamic model (see Fig. 2(c)), but they are unlike those in Fig. 1(c). This phenomenon lasts for a long time in the modeling period (see Fig. 2(c)–(f)). The clogging or queuing phenomenon can be observed near the exit at the top of the facility, while a nearly free-flow traffic state is observed near the exit at the

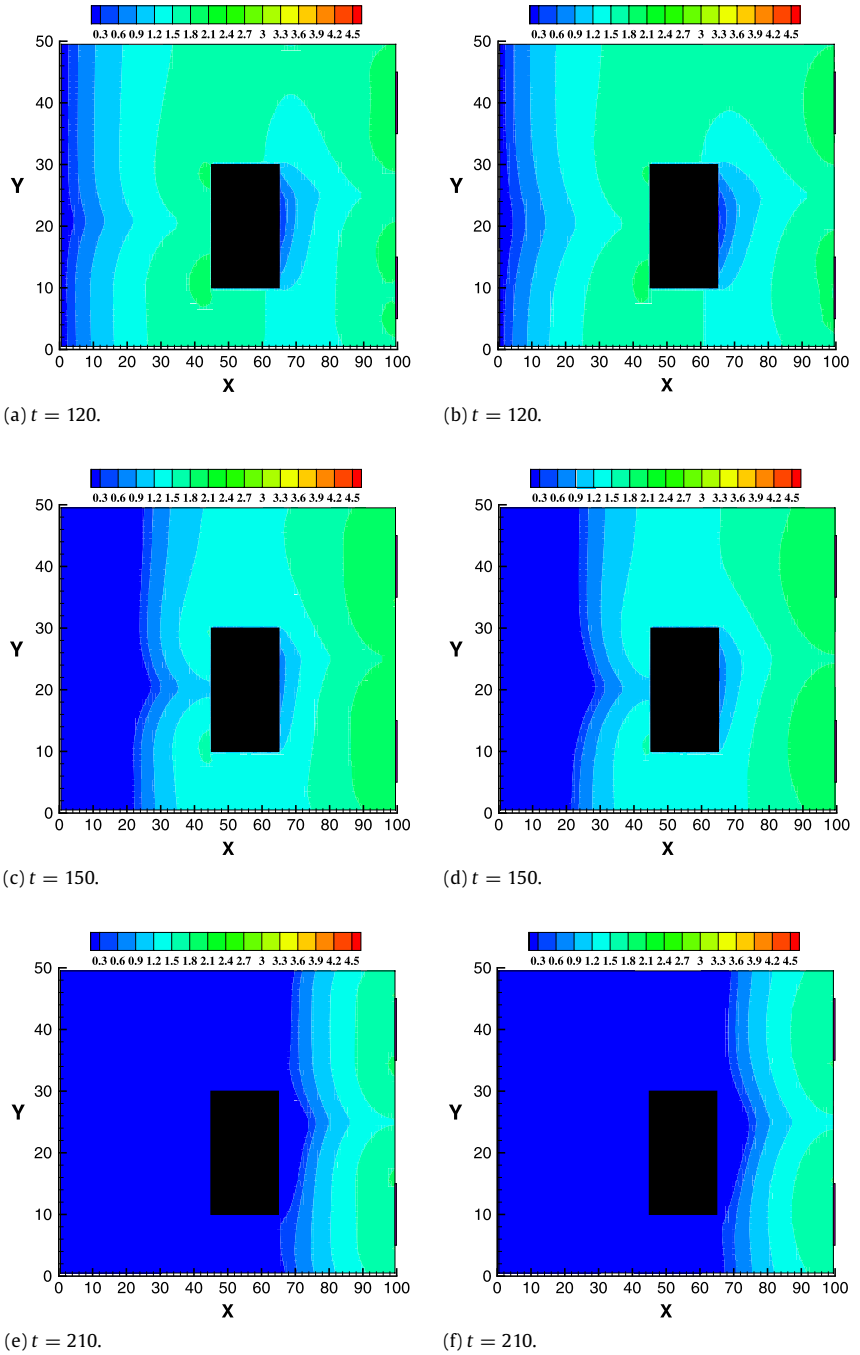

(a) $t = 120$. (b) $t = 120$.

(c) $t = 150$. (d) $t = 150$.

(e) $t = 210$. (f) $t = 210$.

Fig. 4. Density distributions at different times with $\sigma = 5$ based on different models (left: the reactive dynamic model; right: the predictive dynamic model).

bottom of the facility (see Fig. 2(e) and (f)). This is caused by the PDUE path-choice behavior of pedestrians. Based on the two dynamic models, all pedestrians can leave this facility in the modeling period.

The spatial distributions of the desired speeds obtained respectively by the reactive and the predictive dynamic model are illustrated in Fig. 3 at times $t = 120, 150, 180$ with the anticipation degree $\sigma = 0.05$. From Fig. 3, the spatial distributions of the two desired speeds are also different, which further indicates that there exist distinct differences between the RDUE and PDUE path-choice behaviors of pedestrians. The low-speed regions in this figure correspond to the high-density regions in Figs. 1 and 2, respectively, which further demonstrates that the two dynamic models can reproduce the formation of stop-and-go waves. Furthermore, pedestrians slow their speed down at bottlenecks (e.g. near the obstacle and exits) to avoid collisions with other people. When they are far away from these bottlenecks, they speed up to leave the facility quickly.

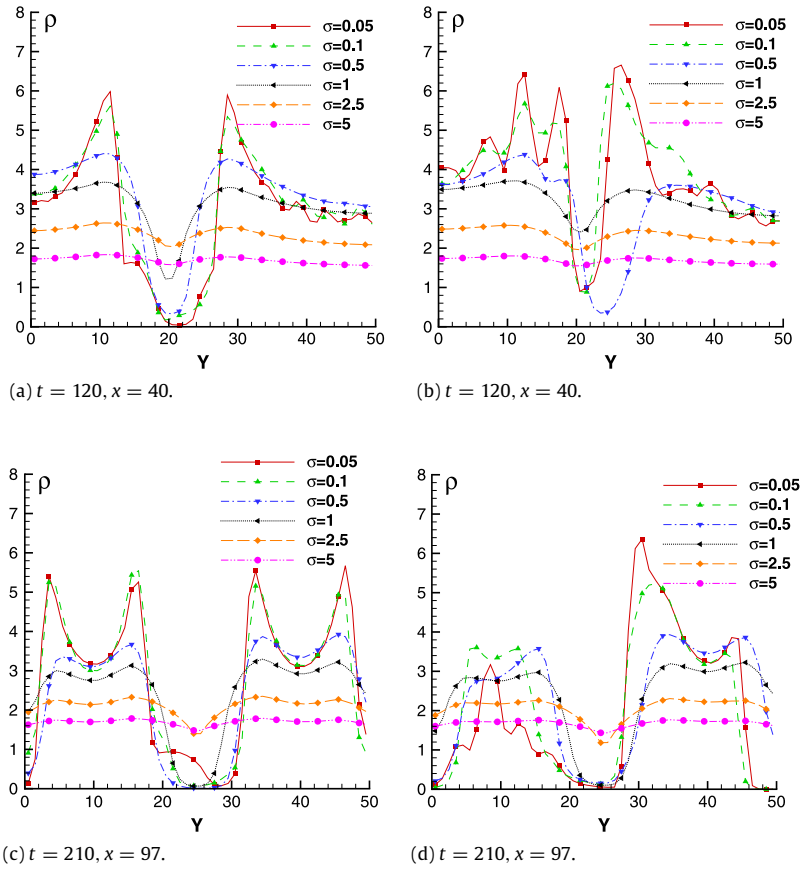

(a) $t = 120, x = 40$. (b) $t = 120, x = 40$.

(c) $t = 210, x = 97$. (d) $t = 210, x = 97$.

Fig. 5. Densities along $x = 40, 97$ based on different models (left: the reactive dynamic model; right: the predictive dynamic model).

Fig. 4 plots the spatial distributions of pedestrian densities obtained respectively by the two dynamic models at times $t = 120, 150, 210$ with the anticipation degree $\sigma = 5 > 0.33$. From this figure, it is observed that the spatial distributions of pedestrian densities are similar at the same time and pedestrian flow is always in a stable and nearly free-flow state in the modeling period. Pedestrians are uniformly distributed in front of the two exits, which accounts for full utilization of the two exits (see Fig. 4(e) and (f)). This also indicates that the strong anticipation consciousness of pedestrians to compression can avoid traffic congestion and thereby reduce traffic accidents.

Fig. 5 shows the density curves based on the two dynamic models along the lines of $x = 40, 97$ at time $t = 120, 210$. When the traffic flow is always in a stable state (i.e. the anticipation degree $\sigma > 0.33$), there are no significant differences between the two models. The pedestrian density decreases with the increase of anticipation consciousness of pedestrians to compression. However, as the anticipation degree σ decreases below the critical value 0.33, traffic instability will occur. The patterns of the local structured clusters are markedly different between the two models especially around the obstacle (see Fig. 5(a) and (b)). For the reactive dynamic model, the spatial distributions of pedestrian density at two exits of the facility are more uniform due to the optimal path-choice strategy of pedestrians based on the available instantaneous information (see Fig. 5(c) and (d)).

5. Conclusions

In this work, we formulate and compare the reactive and predictive dynamic models of pedestrian flow, which describe different path-choice behaviors of pedestrians. The two dynamic models are applied to investigate macroscopic and dynamical features of pedestrians walking in a 2D continuous facility scattered with an obstacle. The reactive dynamic model describes that pedestrians tend to walk along a path with the lowest instantaneous cost based on available instantaneous information. Nevertheless, the predictive dynamic model describes that pedestrians are inclined to choose a path with the lowest actual cost based on predictive traffic information. The algorithm used to solve the two dynamic models is composed of the cell-centered finite volume method, the fast sweeping method and the self-adaptive method of successive averages. Numerical results demonstrate that the two dynamic models have the capability of reproducing the formation of stop-and-go waves and the blocking or queuing effect at bottlenecks (e.g. near the obstacle and exits). The patterns of the local

structured clusters (i.e. stop-and-go waves) are distinctly different at bottlenecks, which are caused by the different path-choice behaviors of pedestrians and the weak anticipation reaction of pedestrians to compression. Furthermore, the strong anticipation consciousness of pedestrians to compression can avoid congestion and thereby reduce accidents in pedestrian traffic.

The physical interactions with rigid objects (e.g. walls) are not taken into account in the reactive and predictive dynamic models, therefore the two models are valid in unbounded domains. Moreover, the function forms of the desired speed, the local cost distribution and equivalent traffic sonic speed (or traffic pressure) utilized in the two models are postulated based on some existing results in vehicular traffic and pedestrian traffic [21,22,34,35,30]. In general, the function forms of these traffic variables are various in different walking environments and appropriate choices of these functions make the macroscopic models for pedestrian dynamics more precise. To describe pedestrian movement more accurately, further works will focus on estimating these interaction forces and function forms based on kinetic theory methods [19,20].

Acknowledgments

This work was supported by the Research Foundation of Southwest University of Science and Technology (No. 10zx7137) and the National Natural Science Foundation of China (Nos. 11202175 and 11372294).

References

[1] A. Kirchner, A. Schadschneider, Simulation of evacuation processes using a bionics-inspired cellular automaton model for pedestrian dynamics, Physica A 312 (2002) 260–276.
[2] R. Alizadeh, A dynamic cellular automaton model for evacuation process with obstacles, Saf. Sci. 49 (2011) 315–323.
[3] R.Y. Guo, New insights into discretization effects in cellular automata models for pedestrian evacuation, Physica A 400 (2014) 1–11.
[4] X.X. Jian, S.C. Wong, P. Zhang, K. Choi, H. Li, X.N. Zhang, Perceived cost potential field cellular automata model with an aggregated force field for pedestrian dynamics, Transp. Res. C 42 (2014) 200–210.
[5] D. Helbing, M. Isobe, T. Nagatani, K. Takimoto, Lattice gas simulation of experimentally studied evacuation dynamics, Phys. Rev. E 67 (2003) 067101.
[6] R.Y. Guo, H.J. Huang, A mobile lattice gas model for simulating pedestrian evacuation, Physica A 387 (2008) 580–586.
[7] E.N.M. Cirillo, A. Muntean, Dynamics of pedestrians in regions with no visibility—a lattice model without exclusion, Physica A 392 (2013) 3578–3588.
[8] X.W. Guo, J.Q. Chen, S.Z. You, J.H. Wei, Modeling of pedestrian evacuation under fire emergency based on an extended heterogeneous lattice gas model, Physica A 392 (2013) 1994–2006.
[9] D. Helbing, P. Molnár, Social force model for pedestrian dynamics, Phys. Rev. E 51 (1995) 4282–4286.
[10] D. Helbing, I. Farkas, T. Vicsek, Simulating dynamical features of escape panic, Nature 407 (2000) 487–490.
[11] P.J. Ma, B.H. Wang, The escape of pedestrians with view radius, Physica A 392 (2013) 215–220.
[12] J.K.K. Yuen, E.W.M. Lee, The effect of overtaking behavior on unidirectional pedestrian flow, Saf. Sci. 50 (2012) 1704–1714.
[13] D. Helbing, L. Buzna, A. Johansson, T. Werner, Self-organized pedestrian crowd dynamics: Experiments, simulations, and design solutions, Transp. Sci. 39 (2005) 1–24.
[14] S.P. Hoogendoorn, W. Daamen, Pedestrian behavior at bottlenecks, Transp. Sci. 39 (2005) 147–159.
[15] N. Bellomo, C. Dogbé, On the modeling of traffic and crowds: A survey of models, speculations, and perspectives, SIAM Rev. 53 (2011) 409–463.
[16] N. Bellomo, A. Bellouquid, D. Knopoff, From the micro-scale to collective crowd dynamics, Multiscale Model. Simul. 11 (2013) 943–963.
[17] J.P. Agnelli, F. Colasuonno, D. Knopoff, A kinetic theory approach to the dynamics of crowd evacuation from bounded domains, Math. Models Methods Appl. Sci. 25 (2015) 109–129.
[18] P. Degond, C. Appert-Rolland, M. Moussaid, J. Pettre, G. Theraulaz, A hierarchy of heuristic-based models of crowd dynamics, J. Stat. Phys. 152 (2013) 1033–1068.
[19] A. Bellouquid, E.D. Angelis, L. Fermo, Towards the modeling of vehicular traffic as a complex system: A kinetic theory approach, Math. Models Methods Appl. Sci. 22 (2012) 1140003.
[20] N. Bellomo, A. Bellouquid, J. Nieto, J. Soler, On the multiscale modeling of vehicular traffic: from kinetic to hydrodynamics, Discrete Contin. Dyn. Syst. Ser. B 19 (2014) 1869–1888.
[21] R.L. Hughes, A continuum theory for the flow of pedestrians, Transp. Res. B 36 (2002) 507–535.
[22] L. Huang, S.C. Wong, M.P. Zhang, C.W. Shu, W.H.K. Lam, Revisiting Hughes' dynamic continuum model for pedestrian flow and the development of an efficient solution algorithm, Transp. Res. B 43 (2009) 127–141.
[23] Y.X. Xia, S.C. Wong, C.W. Shu, Dynamic continuum pedestrian flow model with memory effect, Phys. Rev. E 79 (2009) 066113.
[24] Y.Q. Jiang, T. Xiong, S.C. Wong, C.W. Shu, P. Zhang, M.P. Zhang, W.H.K. Lam, A reactive dynamic continuum user equilibrium model for bi-directional pedestrian flows, Acta Math. Sci. 29B (2009) 1541–1555.
[25] Y.Q. Jiang, S.C. Wong, P. Zhang, R.X. Liu, Y.L. Duan, K. Choi, Numerical simulation of a continuum model for bi-directional pedestrian flow, Appl. Math. Comput. 218 (2012) 6135–6143.
[26] T. Xiong, P. Zhang, S.C. Wong, C.W. Shu, M.P. Zhang, A macroscopic approach to the lane formation phenomenon in pedestrian counter flow, Chinese Phys. Lett. 28 (2011) 108901.
[27] S.P. Hoogendoorn, P.H.L. Bovy, Pedestrian route-choice and activity scheduling theory and models, Transp. Res. B 38 (2004) 169–190.
[28] S.P. Hoogendoorn, P.H.L. Bovy, Dynamic user-optimal assignment in continuous time and space, Transp. Res. B 38 (2004) 571–592.
[29] J. Du, S.C. Wong, C.W. Shu, M.P.Z.T. Xiong, K. Choi, Revisiting Jiang's dynamic continuum model for urban cities, Transp. Res. B 56 (2013) 96–119.
[30] B. Piccoli, A. Tosin, Vehicular Traffic: A Review of Continuum Mathematical Models, in: Encyclopedia of Complexity and Systems Science, vol. 22, Springer, New York, 2009, pp. 9727–9749.
[31] N. Bellomo, C. Dogbé, On the modelling crowd dynamics from scaling to hyperbolic macroscopic models, Math. Models Methods Appl. Sci. 18 (2008) 1317–1345.
[32] D. Helbing, A. Johansson, H.Z. Al-Abideen, The dynamics of crowd disasters: An empirical study, Phys. Rev. E 75 (2007) 046109.
[33] A. Johansson, D. Helbing, H.Z. Al-Abideen, S. Al-Bosta, From crowd dynamics to crowd safety: A video-based analysis, Adv. Complex Syst. 11 (2008) 497–527.
[34] Y.Q. Jiang, P. Zhang, S.C. Wong, R.X. Liu, A higher-order macroscopic model for pedestrian flows, Physica A 389 (2010) 4623–4635.
[35] M. Twarogowska, P. Goatin, R. Duvigneau, Macroscopic modeling and simulations of room evacuation, Appl. Math. Model. 38 (2014) 5781–5795.
[36] E.F. Toro, Riemann Solvers and Numerical Methods for Fluid Dynamics, Springer-Verlag, Berlin, Heidelberg, 1997.
[37] Y.T. Zhang, H.K. Zhao, S. Chen, Fixed-point iterative sweeping methods for static Hamilton–Jacobi equations, Methods Appl. Anal. 13 (2006) 299–320.